Original Research

Coconut Shell Biochar Catalyst Activates Sodium Percarbonate for Rapid Rhodamine B Removal: Efficiency, Influencing Factors, and Mechanisms

Mingya Hao[1, 2], Dongdong Wen[1, 2], Rongbing Fu[1, 2, 3]*

[1]State Key Laboratory of Pollution Control and Resource Reuse, College of Environmental Science and Engineering, Tongji University, Shanghai 200092, China
[2]Centre for Environmental Risk Management & Remediation of Soil & Groundwater, College of Environmental Science and Engineering, Tongji University, Shanghai 200092, China
[3]Shanghai Institute of Pollution Control and Ecological Security, Shanghai 200092, China

Abstract

The efficient activation of sodium percarbonate (SPC) is essential for degrading organic contaminants. Converting biomass into biochar as a multifunctional biocatalyst to accelerate oxidizer activation for water remediation has attracted much attention. In this study, we explored the performance of coconut shell biochar (CSBC) as a catalyst to activate SPC for degrading a model pollutant, rhodamine B (RhB). Optimal CSBC was synthesized via pyrolysis at 700°C for 4 h. In the CSBC/SPC system, the removal efficiency of RhB reached 96.11% within 4 h, which was much higher than that of the SPC system (7.76%). Quenching and electron paramagnetic resonance (EPR) spectroscopy results showed that hydroxyl radicals are crucial reactive oxygen species for RhB removal. Graphitization structures of the material, oxygen-containing functional groups, and persistent free radicals were the dominant factors controlling the activation of SPC by CSBC. Moreover, higher pH (11.72) enhanced the removal of RhB in the CSBC/SPC system; a 30% increase in removal rate was observed. However, anions Cl⁻, SO_4^{2-}, and PO_4^{3-} in water slightly inhibited the removal of RhB. This work provided a new method to activate SPC for the degradation of contaminants in water.

Keywords: sodium percarbonate, coconut shell biochar, degradation, free hydroxyl radical

Introduction

Rapid industrialization has accelerated water environment contamination, posing potential threats to human health [1]. For instance, a previous study indicated that organic contaminants pose serious non-carcinogenic and carcinogenic hazards to humans at a Chinese decommissioned pesticide manufacturing site [2]. Dyes are used in textiles and leather industries; among the wide number of dyes, Rhodamine B (RhB) is a chromophore from the family of xanthene dyes [3]. There are various methods for removing RhB, such as photocatalytic degradation of RhB by a TiO_2-coated activated carbon catalyst [4] and magnetic

---

*e-mail: rongermmfu@163.com
Tel./Fax.: +86 21 65984261

bentonite adsorption of RhB [5]. Nowadays, various physicochemical methods have been extensively employed for the removal of organic contaminants, including adsorption, electrochemical, and advanced oxidation processes (AOPs) [6-8]. In AOPs, various oxidants are used for the degradation of organic contaminants, such as Fenton reagent, Fenton-like reagent, persulfate, and potassium permanganate [9-11]. Among them, Fenton oxidation is commonly used in water remediation due to the presence of reactive oxygen species (ROS) (e.g., hydroxyl radicals (·OH), superoxide radicals ($O_2^{\cdot-}$), singlet line oxygen ($^1O_2$), etc.) [12-14]. ROS are capable of oxidizing organic pollutants until mineralization, *i.e.,* converting organic matter into CO_2, water, and inorganic ions [15-17]. However, the degradation effects of the Fenton system are greatly limited due to the alkaline environment, sludge generation, the difficulty in H_2O_2 storage, and high costs [18, 19]. Therefore, it is of great significance for the selection of oxidants with broader pH compatibility and metal-free catalysts.

Sodium percarbonate ($Na_2CO_3 \cdot 1.5\ H_2O_2$, SPC) has emerged as a novel oxidant and is garnering more attention in AOP remediation [20, 21]. When SPC is dissolved in water, carbonate, water, and oxygen form, as delineated in (Eqs. (1)-(2)). SPC as an alternative to H_2O_2 has various advantages in storage, transportation, and a wide pH range [22]. In addition, SPC is effective in mitigating water acidification and has excellent environmental and biocompatibility. SPC can be used as an oxidizing agent to degrade organic contaminants. However, the efficacy of free radical formation in the atmosphere is hindered without catalytic activation.

$$Na_2CO_3 \cdot 1.5H_2O_2 \rightarrow 2Na^+ + CO_3^{2-} + 1.5H_2O_2 \tag{1}$$

$$2H_2O_2 \rightarrow 2H_2O + O_2 \tag{2}$$
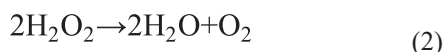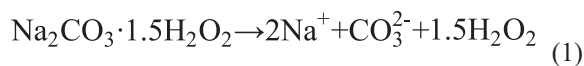
Various methods have been employed for SPC activation, such as ultraviolet (UV), carbon materials, transition metals, heat, and microwave activation [23-26]. To date, previous studies have focused primarily on the activation of SPC by transition metals, iron complexes, and UV [27]. Nevertheless, transition metals induce secondary contamination, and both heat and UV treatments are expensive and impractical for engineering-scale remediation. As an environmentally friendly catalyst, biochar has gained continuous attention due to its low cost and broad application [28]. However, limited studies focus on biochar activating SPC for pollutant removal. Previous studies have indicated that, as a typical biomass material, coconut shell biochar (CSBC) can be used as a catalyst. For example, CSBC doped with α-MnO was used to activate PMS (peroxymonosulfate) for BPA (bisphenol A) degradation [29]. However, the catalytic performance of biochar to activate SPC for contamination removal has been rarely investigated.

Therefore, the main purpose of this study was to: (1) verify the possibility of CSBC activating SPC for the degradation of a target pollutant; (2) compare the catalytic performance of various CSBC; (3) investigate the factors influencing the degradation effects of the CSBC/SPC system; and (4) explore the underlying mechanism of free radical formation in the CSBC/SPC system. The present results could provide a new novel technical method for water remediation.

Materials and Methods

Materials

Rhodamine B (RhB), SPC, concentrated hydrochloric acid (HCl), concentrated sulfuric acid (H_2SO_4), sodium pyrophosphate (H_3PO_4), tert-butyl alcohol (TBA), para-benzoquinone (BQ), and 5, 5-dimethyl-1-pyrroline-N-oxide (DMPO) were obtained from Sinopharm Chemical Reagent Co. Coconut shell raw materials were purchased from Hainan Wenchang.

Biochar Preparation and Characterization

The biochar samples were referred to as YK300, YK500, and YK700 for coconut shell pyrolyzed at 300, 500, and 700ºC for 4h, respectively. The biochar samples were referred to as YK1, YK2, and YK3 for coconut shell pyrolyzed at 700ºC for 1, 2, and 3h, respectively.

The contents of carbon (C) and hydrogen (H) in CSBC were measured using an elemental analyzer (Unicube Vario, Elementar, Germany). The specific surface area of CSBC was determined using the Teller (BET) nitrogen adsorption technique (ASAP 2460, Micromeritics, USA). The surface functional groups of CSBC were identified using Fourier-transform infrared (FTIR) spectroscopy (Nicolet iS20, Thermo Scientific, USA). The microstructure characteristics were analyzed using scanning electron microscopy coupled with energy-dispersive spectroscopy (SEM-EDS) (GeminiSEM 300, ZEISS, Germany). The valence states of carbon and oxygen in CSBC were characterized using X-ray photoelectron spectroscopy (XPS) (5000 VersaProbe III, PHI, Japan). The free radicals in the CSBC/SPC system were detected using electron paramagnetic resonance (EPR) spectroscopy (EMXplus-6/1, Bruker, Germany).

Catalytic Experiments

Batch experiments were performed in flasks containing 250 mL of 20mg/L RhB dye aqueous mixture. The oxidation process was initiated by SPC and CSBC addition. The mixture was agitated at 180 rpm and 25ºC for 4 h. Control experiments without biochar or SPC were also carried out under the same reaction conditions. The efficacy of the CSBC/SPC system in degrading RhB was evaluated following

a comparative study of different reaction systems. Furthermore, radical quenching tests were conducted using different quenchers (TBA, BQ) based on a similar procedure as described above. Samples were collected at predetermined intervals for further analysis. After filtering through 0.45 μm membranes, the sample was analyzed using a UV-Vis spectrophotometer (Cary 3500, Agilent) at a wavelength of 554 nm [30, 31]. The concentration of aqueous RhB was determined using a UV–vis spectrophotometer by measuring its absorbance. After each degradation experiment, CSBC was recovered, washed with deionized water, and dried thoroughly at 80ºC for the subsequent degradation experiment to determine the recyclability and stability of CSBC [32].

The dye decomposition percentage was calculated using Equation (3), where C_0 and C signify the initial and remaining concentration [30]. All the experiments were performed three times to ensure result stability, and the results were reported as mean with standard deviations (SD).

$$(\%) = \frac{C_0 - C}{C_0} \times 100\% \tag{3}$$

Results and Discussion

Characterization of Biochar

Elemental Analysis

Table 1 shows the elemental composition of CSBC prepared under different pyrolysis temperatures and times. When the pyrolysis temperature increased from 300ºC to 700ºC, C contents increased from 70.40% to 83.73%. Conversely, O and contents decreased from 19.6% to 9.00% and from 4.06% to 0.97%, respectively. The mass loss of O and H could be attributed to the cleavage and rupture of weak oxidative bonds within biochar [33]. The H/C ratio was usually related to the aromatic degree of CSBC. The H/C ratio increased as pyrolysis temperature increased, indicating a significantly higher aromatic degree of CSBC. In addition, dehydration, decarboxylation, and demethylation might enhance the carbonization and

stability of biochar [34, 35]. A loss of C and H elements was observed in CSBC with prolonged time, due to the release of gases such as methane (CH_4) and hydrogen (H_2) [35, 36]. Conversely, N content remained relatively constant.

The BET Analysis of CSBC

Fig. 1 presents N_2 adsorption–desorption isotherms of CSBC. The N_2 adsorption curves of CSBC were consistent with Type I isotherms, and the hysteresis loop type belonged to type H4, indicating the presence of lots of microporous structures in CSBC. The surface area and pore size of CSBC were 314.5231 m²/g and 2.1747 nm for YK1h, 339.7825 m²/g and 3.4086 nm for YK2h, 500.7433 m²/g and 3.0610 nm for YK3h, 575.6408 m²/g and 3.4757 nm for YK700, 1.8508 m²/g and 53.0390 nm for YK300, 117.7411 m²/g and 4.9598 nm for YK500, respectively. These results indicated that with increasing pyrolysis temperature and time, the specific surface area of CSBC progressively increased [37], which increased active sites and enhanced activation efficiency.

The microstructure characteristics of CSBC

Fig. 1 shows SEM micrographs of CSBC. YK700 was characterized by fine porosity with roughened surface texture and stratified morphology. The YK700 after catalysis retained the basic structure of the pristine biochar, but became more brittle and porous with increased pore size and damaged surface structure. Compared with the pristine YK700, the surface structure of the used YK700 was damaged; the previous continuous layered structure was transformed into a disintegrated discrete structure. Moreover, YK300 and YK500 lacked definitive regularity and showed irregular arrangements with heterogeneous and macropore structures. In contrast, YK700 showed higher graphitization and a larger specific surface area, which was conducive to electron transfer. Many previous studies have reported that as the charge transfer medium, the graphitized structure of CSBC significantly contributed to electron transfer from oxidants to organic contaminants [38]. Therefore, compared to YK300 and YK500, YK700 might have better catalytic ability.

Table 1. The contents of C, O, H, and N in CSBC under different pyrolysis temperatures and times.

Biochar	Pyrolysis temperature	Pyrolysis time	N (%)	C (%)	H (%)	O (%)
YK300	300ºC	4 h	0.17	70.40	4.06	19.60
YK500	500ºC	4 h	0.16	85.36	2.90	10.85
YK1h	700ºC	1 h	0.19	91.51	1.29	6.85
YK2h	700ºC	2 h	0.16	85.20	1.18	9.66
YK3h	700ºC	3 h	0.17	84.88	1.10	7.78
YK700	700ºC	4 h	0.18	83.73	0.97	9.00

CSBC had lots of O-containing functional groups, which were also considered to be the main catalytic active sites [39]. Both the pyrolysis temperature and time were the key parameters influencing OFG formation [40]. Fig. 1g) and h) show FTIR spectroscopy of CSBC. As shown in Fig. 2e), the stretching vibration at 3432.73 cm^{-1} belonged to -OH groups, while the stretching vibration at 1068.10 cm^{-1} showed the presence of C-O bonds, indicating the presence of -OH groups in CSBC [41, 42]. The peak at 1612.74 cm^{-1} might be related to the vibration of -C=C. In addition, the peak at 1630 cm^{-1} might be due to the stretching vibration of -C=O. The disappearance of the infrared peak for C=O in YK700 indicated that -C=O might be an essential functional group in SPC activation by CSBC. As shown in Table 1, the peak at 2230-2358 cm^{-1} may be due to the stretching vibration of -C≡N, due to 18% of N in CSBC. The peak at 1385.12 cm^{-1} showed that CSBC contained -OH bonds, which could produce •OH from H$_2$O$_2$ by electron transfer [43]. Previous studies have shown that some OFGs had functional oxidation and reduction effects (e.g., quinones or phenolic hydroxyl groups), which could transfer electrons to cooperatively catalyze oxidation [44]. The results showed that YK700 has abundant OFGs and more active sites with stronger peak intensity, indicating excellent catalytic performance.

The XPS Analysis of CSBC

Fig. 1i) and j) show the XPS spectra of CSBC. Three distinct peaks of the C1s spectrum of YK700 at 284.8 eV, 287.8 eV, and 292.7 eV corresponded to -C=C, -C=O, and π-π*, respectively. The results indicated that pyrolytic YK700 showed a graphitic carbon structure. In the O 1s spectrum, two peaks at 530.8 eV and 532.6 eV corresponded to -C=O and -C-O, respectively. Moreover, it was observed that the percentage of -C=O peak areas decreased in the C 1s spectrum, suggesting that -C=O groups were involved in the reaction.

The Selectivity of CSBC Based on Their Catalytic Performance

Adsorption experiments were performed to explore the possibility of SPC activation by CSBC for RhB degradation, as depicted in Fig. 2a); the adsorption capacities for YK300, YK500, and YK700 were 2.07%, 1.01%, and 16.02%, respectively. Among them, YK700 showed the highest adsorption capacities, due to the larger specific surface area and more abundant porous structure. The increase in temperatures enhanced adsorption performance, due to the formation and
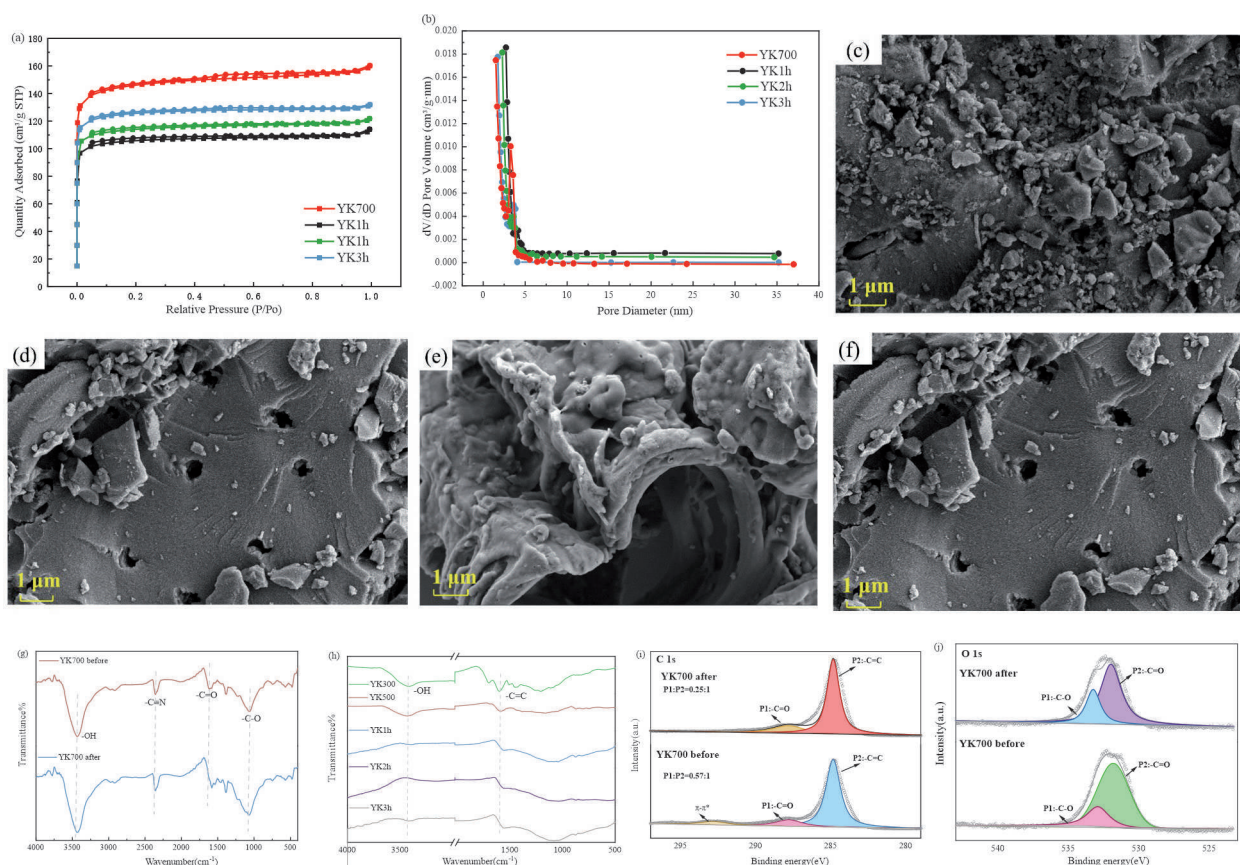

Fig. 1. N$_2$ adsorption–desorption isotherm a); pore size distribution curve b); SEM images of YK300 c), YK500 d), YK700 e), and YK700 after catalysis f); FTIR of YK700 g) and after catalysis h); YK700 about high-resolution XPS spectra of C 1s i) and O 1s j).

development of pores in CSBC [45]. In a single SPC system, the degradation efficiency of RhB was 7.76% within 240 min. In the YK300/SPC system, the degradation efficiency of RhB decreased to 3.57% within 240 min. Conversely, in the YK500/SPC and YK700/SPC systems, the degradation efficiency of RhB increased to 4.81% and 45.01% within 60 min, respectively, and reached 11.64% and 96.11% after 240 min, respectively. YK500/SPC systems showed a slight increase in the degradation efficiency of RhB compared to a single SPC system. Nevertheless. The removal efficiency of RhB in the CSBC/SPC system was comparable to what AOPs. For the 700YK/SPC system, the degradation efficiency of RhB increased significantly by 88.35% compared to a single SPC. The volatilization of cellulose and lignin from the CSBC might enhance the degradation performance of RhB, which likely improved interaction between active sites on the CSBC surface and SPC and thus resulted in a higher generation of •OH radicals for RhB degradation. Furthermore, CSBC volatilization led to an increase in specific surface area and porosity [36].

Fig. 2b) illustrates the degradation performance of RhB by SPC activation by CSBC. The degradation efficiency of RhB was 8.5% for YK1h, 8.57% for YK2h, and 16.23% for YK3h, respectively. The extended pyrolysis time enhanced RhB degradation. The kinetic degradation test of RhB was conducted to determine the inherent activity of CSBC. Fig. 2c) and d) present

the kinetic degradation results of RhB. The degradation kinetics of RhB could be better fitted by the pseudo-first-order kinetic model. Overall, YK700 exhibited the best catalytic performance, compared with other CSBCs, since it might have more active sites [46].

YK700 almost completely degraded RhB after 4 h of reaction. CSBC pyrolyzed at 700°C for 4 h demonstrated the best catalytic performance in the RhB degradation by SPC. Therefore, YK700 was used in all the subsequent tests.

Key Factors Affecting RhB Degradation in the YK700/SPC System

Effect of CSBC Concentration

Fig. 3a) shows the RhB degradation results with CSBC dosages. CSBC dosages had significant influences on the degradation efficiency of RhB by SPC. Fig. 3b) and c) present the degradation kinetics results of RhB in the CSBC/SPC system. The degradation kinetics data of RhB could be better fitted by pseudo-first-order kinetics at lower CSBC dosages, while that could be better fitted by pseudo-second-order kinetics at higher CSBC dosages. Intriguingly, the degradation rates of RhB at 2 g/L of CSBC were 20 times higher than those at 1 g/L of CSBC. The degradation rates of RhB increased rapidly, probably due to the limited SPC content. Therefore, the number of active sites on the CSBC
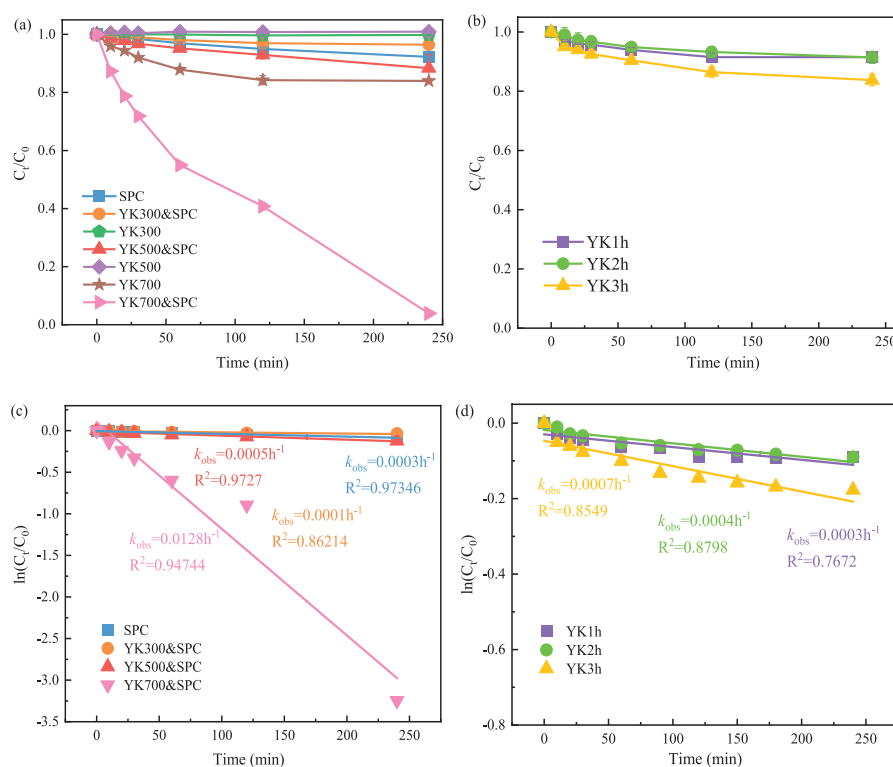

Fig. 2. Degradation curves of RhB by SPC, which is catalyzed by CSBC at various pyrolysis temperatures a); Degradation curves at varying pyrolysis durations b); First-order kinetics at different pyrolysis temperatures c); First-order kinetics across various pyrolysis durations d). Experimental conditions: [RhB] = 20 mg/L, [SPC] = 1 g/L, [BC] = 1 g/L, time= 240 min, and T = 25ºC.
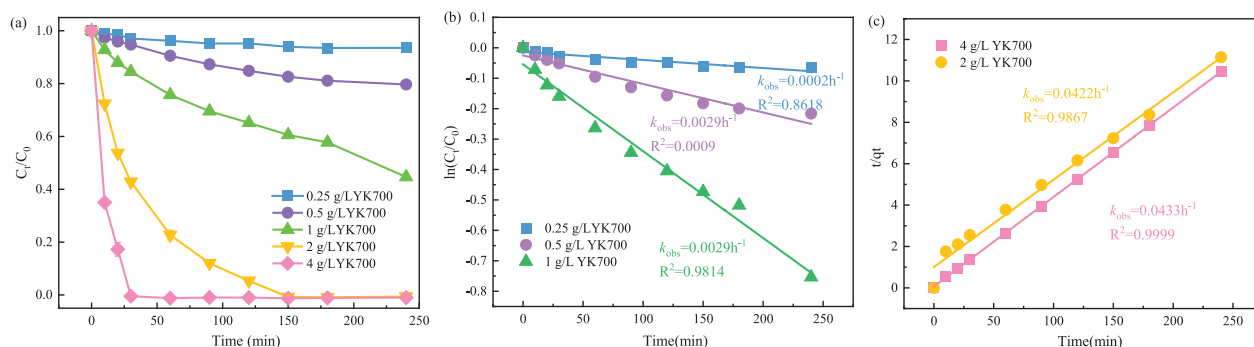
Fig. 3. Degradation curves of RhB by YK700/SPC at different catalyst concentrations a), kinetics of the YK700/SPC pseudo-primary reaction at different concentrations b), kinetics of the YK700/SPC pseudo-secondary reaction, and c), experimental conditions: [RhB] = 20 mg/L, [SPC] = 1 g/L, time = 240 min, and T = 25ºC.

surface dominated RhB degradation. The C=O groups and defect structures on the YK700 surface could serve as catalytic active sites to promote the generation of free radicals [47].

Effect of SPC Concentration

Fig. 4 shows the RhB degradation results with SPC concentration. As shown in Fig. 4a), the degradation efficiency of RhB increased from 49.8 to 99.63% as the SPC concentration increased from 0.25 to

4 g/L, indicating a positive correlation between SPC concentration and RhB degradation. The increase in SPC concentration enhanced the formation of more surface radicals in the solution, resulting in higher RhB degradation efficiency [48]. However, the degradation efficiency did not significantly increase at the SPC concentration of 2 g/L compared to that of 1 g/L. The results might be because excess SPC under the same CSBC concentration did not generate lots of •OH radicals. Therefore, the optimal dosage ratio of SPC to YK700 was 1:2, based on the economic perspective.
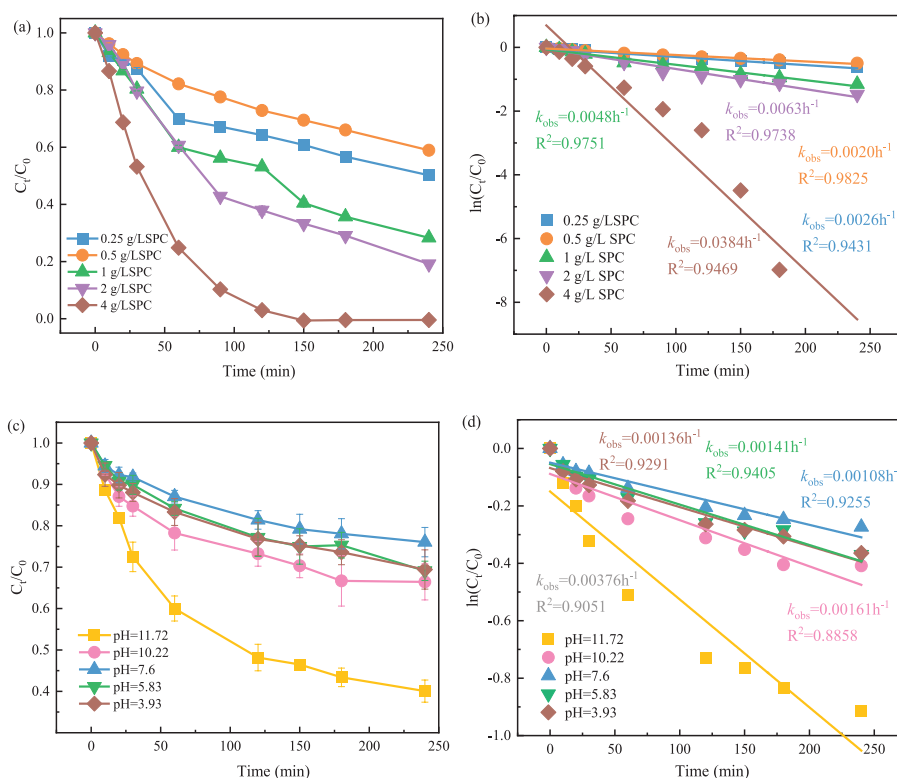

Fig. 4. RhB degradation curves by different concentrations of oxidants a); Kinetics of oxidant-catalyzed SPC primary reactions b). Experimental conditions: [RhB] = 20 mg/L, [BC] = 1 g/L, time = 240 min, and T = 25ºC, RhB's degradation curves of SPC catalyzed by CSBC at different pH c), Kinetics of SPC-catalyzed primary reaction of CSBC at different pH d). Experimental conditions: [RhB] = 20 mg/L, [SPC] = 1 g/L, [BC] = 1 g/L, time = 240 min, and T = 25ºC.

Effect of pH

Fig. 4c) shows the RhB degradation results with pH. The YK700/SPC system exhibited good degradation efficiency for RhB in an alkaline environment. The degradation efficiency of RhB at pH = 11.72 is higher than that at pH = 3.93 by 29.44%. This might be because SPC activation by CSBC resulted in the formation of •OH and H^+. The continuous consumption of H^+ in an alkaline environment increased the number of free radicals and thus enhanced RhB degradation [49]. In addition, RhB is a cationic dye and is positively charged in an acidic environment. In alkaline environments, the carboxylate group of RhB dye is deprotonated to the negatively charged −COO− state [50]. Under alkaline conditions, the CSBC/SPC system showed increased interaction with RhB and enhanced SPC generation for •OH [51]. The carbonates contained in SPC change to bicarbonate in an acidic environment. Bicarbonate has a significant inhibitory effect on •OH, so RhB degradation is significantly reduced in acidic environments [52].

Effect of RhB Concentrations

Fig. 5a) illustrates the RhB degradation results with RhB concentrations. An increase in RhB concentration resulted in a decrease in the degradation efficiency of RhB. The degradation efficiency of RhB was relatively low at the initial RhB concentration of 30 mg/L, whereas that notably increased at the initial RhB concentrations of 20 mg/L (69.56%) and 10 mg/L (100%), respectively.

Effect of Inorganic Anions

Fig. 5c) illustrates the RhB degradation results with inorganic anions. In the presence of Cl^-, SO_4^{2-}, and PO_4^{3-}, the degradation efficiency of RhB was 54.59%, 59.16%, and 51.17%, respectively. Without inorganic anions, the degradation efficiency of RhB was 73.75%. These results indicated that Cl^-, SO_4^{2-}, and PO_4^{3-} could inhibit RhB degradation, possibly because the inorganic anions in reaction with free radicals led to radical consumption [53].

CSBC Reusability

Fig. 5d) shows the RhB degradation results with CSBC reusability. The degradation efficiency of RhB decreased by 56% from the 1st to the 5th cycles. However, CSBC could still effectively degrade RhB, verifying the stability and recyclability of the CSBC. The results were probably because the decomposition intermediates on the CSBC surface inhibited the interaction between CSBC and SPC [54].
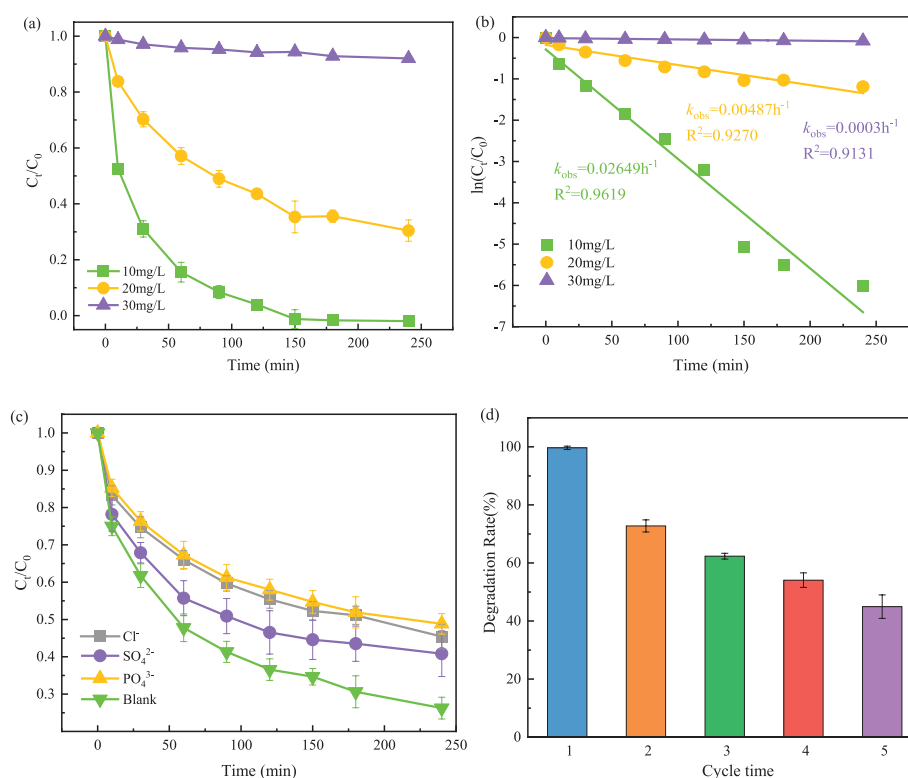

Fig. 5. CSBC catalyzed SPC degradation profiles of RhB at different initial concentrations a); Kinetics of the CSBC-catalyzed SPC primary reaction with different initial concentrations of RhB b). Experimental conditions: [SPC] = 1 g/L, [BC] = 1 g/L, time = 240 min, and T = 25ºC. Degradation curves in the presence of different anions [RhB] = 20 mg/L, [SPC] = 1g/L, [BC] = 1g/L, [anions] = 20 mM/L c); Number of recycling times after YK700 catalysis [RhB] = 20 mg/L, [SPC] = 1 g/L, [BC] = 1 g/L, T=25ºC d).
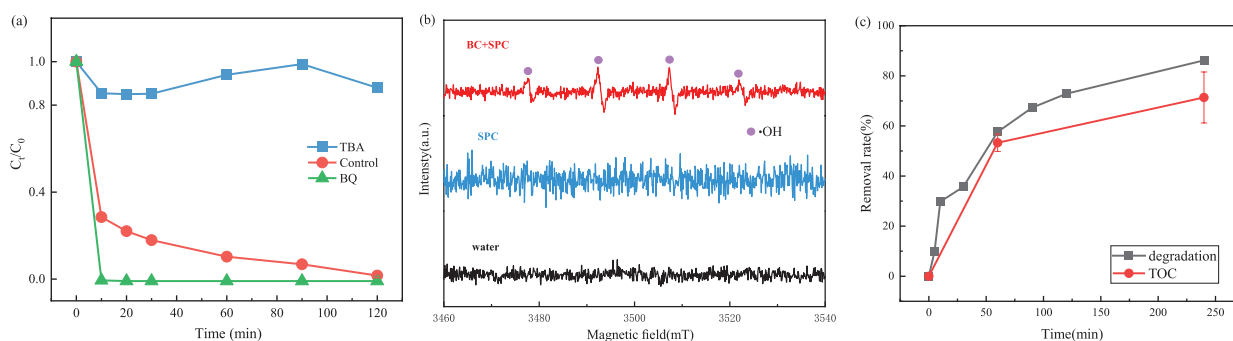
Fig. 6. Effect of quenchers on RhB removal a); Electron paramagnetic resonance (EPR) spectra of radical adducts trapped by 5,5-dimethyl-1-pyrroline N-oxide (DMPO) of the SBC catalyst b); The change diagram of degradation and TOC in the CSBC/SPC reaction system at different reaction times: initial [RhB] = 20 mg/L, [SPC] = 1 g/L, [BC] = 1 g/L.

The Possible Catalytic Mechanism of SPC Activation by CSBC
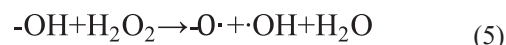
In YK700/SPC, the degradation efficiency of RhB was 98.37%. As a superoxide radical ($O_2^{\bullet-}$) scavenger, BQ addition led to a complete removal of 100% within 120 min, due to the established role of $O_2^{\bullet-}$ as an intermediate in the reaction system. OFGs in CSBC could facilitate electrons transferred to dissolved oxygen, resulting in superoxide radicals ($O_2^{\bullet-}$) formation. These $O_2^{\bullet-}$ radicals could react with H^+ to form H_2O_2, which could be further converted into $\bullet OH$. Due to $O_2^{\bullet-}$ consumption, BQ addition led to the formation of more $\bullet OH$ radicals and further destroyed the RhB degradation equilibrium [55, 56].

As a $\bullet OH$ quenching agent, TBA was introduced into the CSBC/SPC system, resulting in the RhB degradation efficiency of 12.01% with 120 min. TBA addition significantly inhibited RhB degradation, confirming that the main free radical in the CSBC/SPC system was $\bullet OH$, which was consistent with previous studies [31]. Furthermore, the EPR spectrum (Fig. 6b) demonstrated that the CSBC/SPC generated an $\bullet OH$ signal. In contrast, no discernible peak was observed in the single SPC system, indicating that the main active radical in RhB oxidation was $\bullet OH$ [57].

In addition, the partial degradation of RhB after TBA addition suggested the potential role of CSBC as an electron transfer medium. The XPS spectra indicated the presence of sp^2 hybridized carbon π-π^* transitions in YK700. Previous studies have shown that π-π^* stacking structures benefited from the graphitized structure of biochar and enhanced long-distance electron transfer [58]. The disappearance of the π-π^* signal peak in the C1s spectra indicated that YK700 enhanced electron transfer between SPC and RhB and thus increased RhB degradation efficiency. These results indicated that YK700 might serve as an electron transfer medium, enhancing the electron transfer between SPC and RhB through a non-radical pathway. However, the non-radical pathway was not dominant based on the results of quenching tests. RhB degradation was primarily facilitated by the attack of $\bullet OH$ radicals.

Based on the above analysis, the CSBC/SPC system likely enhanced RhB degradation through the $\bullet OH$ radical. Graphitized carbon in CSBC showed an enhanced potential for electron acceptance, which might play a key role in SPC activation [59]. The active sites for SPC activation and catalysis mainly included defects, oxygen-containing functional groups, and the graphite-carbon structure of CSBC [60, 61]. The RhB degradation mechanism in the YK700/SPC system might involve: (1) The transfer of electrons from surface functional groups (e.g., -COOH, -OH, and -C=O) on CSBC to SPC generated $\bullet OH$ radicals, as shown in Equations (4)-(6) [62]. (2) Defect structures and persistent free radicals could activate SPC to generate $\bullet OH$ radicals [63].

In order to further explain the degradation of RhB in the reaction system, the degradation rate and TOC in the reactive solution were detected. As shown in Fig. 6c), when the reaction time increases, the degradation rate of RhB solution and the removal rate of TOC increase gradually. This finding shows that the CSBC/SPC system effectively removes RhB and mineralizes into CO_2 and H_2O.

$$-COOH+H_2O_2 \rightarrow -COO+\cdot OH+H_2O \quad (4)$$

$$-OH+H_2O_2 \rightarrow -O\cdot+\cdot OH+H_2O \quad (5)$$

$$-C=O+H_2O_2 \rightarrow -COOH+\cdot OH \quad (6)$$

Conclusion

A simple method for preparing a CSBC free of metal catalysts was proposed and applied as an SPC activator to eliminate contaminations. The use of YK700 in SPC activation was more advantageous than that of the YK300 and YK500 due to faster and higher RhB removal. The process exhibited satisfactory activity toward RhB degradation over the alkaline environment, and the degradation increased by 29.44% compared with an acidic solution. The addition of Cl^-, SO_4^{2-},

and PO_4^{3-} anions to the system showed that all these anions inhibited the degradation of RhB. EPR results indicated that the primary free radicals involved in the degradation of RhB in the system are •OH. CSBC primarily activated SPC to generate reactive oxygen species for pollutant degradation through radical pathways, involving active sites like OFGs, PFRs, and defect structures on its surface. Furthermore, non-radical pathways in YK700/SPC also promoted electron transfer for the degradation of pollutants. Overall, the results suggested that the CSBC/SPC system can effectively treat groundwater contamination. This study provided an efficient and green degradation pathway for the treatment of recalcitrant organic in the groundwater and offered new strategies for the resource utilization of coconut shell waste.

Acknowledgment

Conflict of Interest

The authors declare that they have no known competing financial interests or personal relationships that could have appeared to influence the work reported in this paper.

Reference

1. LI P., KARUNANIDHI D., SUBRAMANI T., SRINIVASAMOORTHY K. Sources and Consequences of Groundwater Contamination. Archives of Environmental Contamination and Toxicology, **80** (1), 1, **2021**.

2. LINZHI Z., QIAN D., XUANLIANG D., YIJUN Y, LIJING D. Health Risk Assessment of Groundwater Volatile Organic Compounds Contamination at an Abandoned Pesticide Production Site. Environmental Monitoring Management and Technology, **26** (05), 24, **2014**.

3. BANAZADEH A., SALIMI H., KHALEGHI M., SHAFIEI-HAGHIGHI S. Highly efficient degradation of hazardous dyes in aqueous phase by supported palladium nanocatalyst – A green approach. Journal of Environmental Chemical Engineering, **4** (2), 2178, **2016**.

4. LI Y., SUN S., MA M., OUYANG Y., YAN W. Kinetic study and model of the photocatalytic degradation of rhodamine B (RhB) by a TiO_2-coated activated carbon catalyst: Effects of initial RhB content, light intensity and TiO_2 content in the catalyst. Chemical Engineering Journal, **142** (2), 147, **2008**.

5. WAN D., LI W., WANG G., CHEN K., LU L., HU Q. Adsorption and heterogeneous degradation of rhodamine B on the surface of magnetic bentonite material. Applied Surface Science, **349**, 988, **2015**.

6. BAEK K., MAO X., CIBLAK A., ALSHAWABKEH AKRAM. N. Green Remediation of Soil and Groundwater by Electrochemical Methods. GeoCongress 2012 Roman D. Hryciw, Adda Athanasopoulos-Zekkos, Nazli Yesiller, ASCE Bookstore: USA, 4348, **2012**.

7. DING D., JIANG D., ZHOU Y., XIA F., CHEN Y., KONG L., WEI J., ZHANG S., DENG S. Assessing the environmental impacts and costs of biochar and monitored natural attenuation for groundwater heavily contaminated with volatile organic compounds. Science of The Total Environment, **846**, 157316, **2022**.

8. DONG S., SHEN X., GUO Q., CHENG H., GIANNAKIS S., HE Z., WANG L., WANG D., SONG S., MA J. Valorization of soybean plant wastes in preparation of N-doped biochar for catalytic ozonation of organic contaminants: Atrazine degradation performance and mechanistic considerations. Chemical Engineering Journal, **472**, 145153, **2023**.

9. WANG Y, ZHENG K, GUO H, TIAN L, HE Y, WANG X, ZHU T, SUN P, LIU Y. Potassium permanganate-based advanced oxidation processes for wastewater decontamination and sludge treatment: A review. Chemical Engineering Journal, **452**, 139529, **2023**.

10. GAO Y., ZOU D. Efficient degradation of levofloxacin by a microwave–3D $ZnCo_2O_4$/activated persulfate process: Effects, degradation intermediates, and acute toxicity. Chemical Engineering Journal, **393**, 124795, **2020**.

11. PAN Y., ZHANG Y., HOU M., XUE J., QIN R., ZHOU M., ZHANG Y. Properties of polyphenols and polyphenol-containing wastewaters and their treatment by Fenton/Fenton-like reactions. Separation and Purification Technology, **317**, 123905, **2023**.

12. WANG L., LIU S., LU J., YUAN Z., GAO D., LI Y. Construction of ZnFe2O4/g-C3N4 nanocomposite catalyst for degradation of organic compound through photodegradation and heterogeneous Fenton oxidation. Materials Today Sustainability, **24**, 100514, **2023**.

13. CHO E-J., KANG J-K., LEE C-G., BAE S., PARK S-J. Use of thermally activated Fenton sludge for Cd removal in zinc smelter wastewater: Mechanism and feasibility of Cd removal. Environmental Pollution, **334**, 122166, **2023**.

14. FURMAN O., LAINE D.F., BLUMENFELD A., TEEL A. L., SHIMIZU K., CHENG I.F., WATTS R.J. Enhanced Reactivity of Superoxide in Water-Solid Matrices. Environmental Science & Technology, **43** (5), 1528, **2009**.

15. BARHOUMI N., OTURAN N., OLVERA-VARGAS H., BRILLAS E., GADRI A., AMMAR S., OTURAN M. A. Pyrite as a sustainable catalyst in electro-Fenton process for improving oxidation of sulfamethazine. Kinetics, mechanism, and toxicity assessment. Water Research, **94**, 52, **2016**.

16. PANIZZA M., CERISOLA G. Direct and mediated anodic oxidation of organic pollutants. Chemical Reviews, **109** (12), 6541, **2009**.

17. RODRIGO M.A., OTURAN M.A., OTURAN N. Electrochemically assisted remediation of pesticides in soils and water: A review. Chemical Reviews, **114** (17), 8720, **2014**.

18. MEI W., LI D., XU H., ZAN J., SUN L., LI Q., ZHANG B., WANG Y., XIA D. Effect of electronic migration of MIL-53(Fe) on the activation of peroxymonosulfate under visible light. Chemical Physics Letters, **706**, 694, **2018**.

19. WANG H., ZHANG L., HU C., WANG X., LYU L., SHENG G. Enhanced degradation of organic pollutants over Cu-doped LaAlO3 perovskite through heterogeneous

Fenton-like reactions. Chemical Engineering Journal, **332**, 572, **2018**.

20. CHENG X., LIAN J., REN Z., HOU C., JIN Y., ZHANG L., ZHU X., LUO C., WU D., LIANG H. Coupling sodium percarbonate (SPC) oxidation and coagulation for membrane fouling mitigation in algae-laden water treatment. Water Research, **204**, 117622, **2021**.

21. GAO J., SONG J., YE J., DUAN X., DIONYSIOU D.D., YADAV J.S., NADAGOUDA M.N., YANG L., LUO S. Comparative toxicity reduction potential of UV/sodium percarbonate and UV/hydrogen peroxide treatments for bisphenol A in water: An integrated analysis using chemical, computational, biological, and metabolomic approaches. Water Research, **190**, 116755, **2021**.

22. YUE-HUA Z., CHUN-MEI X., CHANG-HONG G. Application sodium percarbonate to oxidative degradation trichloroethylene contamination in groundwater. Procedia Environmental Sciences, **10**, 1668, **2011**.

23. LIU X., HE S., YANG Y., YAO B., TANG Y., LUO L., ZHI D., WAN Z., WANG L., ZHOU Y.A review on percarbonate-based advanced oxidation processes for remediation of organic compounds in water. Environmental Research, **200**, 111371, **2021**.

24. SINDELAR H.R., BROWN M.T., BOYER T.H. Evaluating UV/H$_2$O$_2$, UV/percarbonate, and UV/perborate for natural organic matter reduction from alternative water sources. Chemosphere, **105**, 112, **2014**.

25. LYU H., ZHANG Q., SHEN B. Application of biochar and its composites in catalysis. Chemosphere, **240**, 124842, **2020**.

26. ASSILA O., VILAÇA N., BERTÃO A.R., FONSECA A.M., PARPOT P., SOARES O.S.G.P., PEREIRA M.F.R., BALTAZAR F., BAÑOBRE-LÓPEZ M., NEVES I.C. Optimization of iron-ZIF-8 catalysts for degradation of tartrazine in water by Fenton-like reaction. Chemosphere, **339**, 139634, **2023**.

27. LI L., HUANG J., HU X., ZHANG S., DAI Q., CHAI H., GU L. Activation of sodium percarbonate by vanadium for the degradation of aniline in water: Mechanism and identification of reactive species. Chemosphere, **215**, 647, **2019**.

28. JING X-R., WANG Y-Y., LIU W-J., WANG Y-K., JIANG H. Enhanced adsorption performance of tetracycline in aqueous solutions by methanol-modified biochar. Chemical Engineering Journal, **248**, 168, **2014**.

29. FANG X., WU Y., XU L., GAN L. Fast removal of bisphenol A by coconut shell biochar incorporated α-MnO$_2$ composites via peroxymonosulfate activation. Journal of Water Process Engineering, **49**, 103071, **2022**.

30. PATIAL S., SONU, THAKUR S., VAN LE Q., AHAMAD T., SINGH P., NGUYEN V-H., KHAN A.A.P., HUSSAIN C.M., RAIZADA P. Facile synthesis of Co, Fe-bimetallic MIL-88A/microcrystalline cellulose composites for efficient adsorptive and photo-Fenton degradation of RhB dye. Journal of the Taiwan Institute of Chemical Engineers, **153**, 105189, **2023**.

31. MO Z., LI C., ZHANG Y., REN J., ZHU Z., LIANG J., YE M., ZHU Z., ZHU S., YANG W., XU Z., WONG J.W.C. Ball-milled pyrite@biochar induced percarbonate activation for sustainable degradation of antibiotic norfloxacin at inherent pH environment. Separation and Purification Technology, **335**, 126202, **2024**.

32. CAI F., SUN C., SUN Z., LAI Y., DING H. Sulfur-functionalized CoMn$_2$O$_4$ as a Fenton-like catalyst for the efficient rhodamine B degradation. Applied Surface Science, **623**, 157044, **2023**.

33. DEMIRBAS A. Effects of temperature and particle size on bio-char yield from pyrolysis of agricultural residues. Journal of Analytical and Applied Pyrolysis, **72** (2), 243, **2004**.

34. KRZESIŃSKA M., PILAWA B., PUSZ S., NG J. Physical characteristics of carbon materials derived from pyrolysed vascular plants. Biomass and Bioenergy, **30** (2), 166, **2006**.

35. WANG Z., CAO J., WANG J. Pyrolytic characteristics of pine wood in a slowly heating and gas sweeping fixed-bed reactor. Journal of Analytical and Applied Pyrolysis, **84** (2), 179, **2009**.

36. SULIMAN W., HARSH J.B., ABU-LAIL N.I., FORTUNA A-M., DALLMEYER I., GARCIA-PEREZ M. Influence of feedstock source and pyrolysis temperature on biochar bulk and surface properties. Biomass and Bioenergy, **84**, 37, **2016**.

37. KLOSS S., ZEHETNER F., DELLANTONIO A., HAMID R., OTTNER F., LIEDTKE V., SCHWANNINGER M., GERZABEK M.H., SOJA G. Characterization of Slow Pyrolysis Biochars: Effects of Feedstocks and Pyrolysis Temperature on Biochar Properties. Journal of Environmental Quality, **41** (4), 990, **2012**.

38. ZHONG Q., LIN Q., HE W., FU H., HUANG Z., WANG Y., WU L. Study on the nonradical pathways of nitrogen-doped biochar activating persulfate for tetracycline degradation. Separation and Purification Technology, **276**, 119354, **2021**.

39. SHAO P., TIAN J., YANG F., DUAN X., GAO S., SHI W., LUO X., CUI F., LUO S., WANG S. Identification and Regulation of Active Sites on Nanodiamonds: Establishing a Highly Efficient Catalytic System for Oxidation of Organic Contaminants. Advanced Functional Materials, **28** (13), 1705295, **2018**.

40. GODVIN SHARMILA V., KUMAR TYAGI V., VARJANI S., RAJESH BANU J. A review on the lignocellulosic derived biochar-based catalyst in wastewater remediation: Advanced treatment technologies and machine learning tools. Bioresource Technology, **387**, 129587, **2023**.

41. KEMMOU L., FRONTISTIS Z., VAKROS J., MANARIOTIS I.D., MANTZAVINOS D. Degradation of antibiotic sulfamethoxazole by biochar-activated persulfate: Factors affecting the activation and degradation processes. Catalysis Today, **313**, 128, **2018**.

42. ZHAO Y., YUAN X., LI X., JIANG L., WANG H. Burgeoning prospects of biochar and its composite in persulfate-advanced oxidation process. Journal of Hazardous Materials, **409**, 124893, **2021**.

43. INYANG M., DICKENSON E. The potential role of biochar in the removal of organic and microbial contaminants from potable and reuse water: A review. Chemosphere, **134**, 232, **2015**.

44. XIAO X., REN Y., LEI Y., LI X., GUO H., ZHANG C., JIAO Y. Jasmine waste derived biochar as green sulfate catalysts dominate non-free radical paths efficiently degraded tetracycline. Chemosphere, **339**, 139610, **2023**.

45. YANG F., LI W., OU R., LU Y., DONG X., TU W., ZHU W., WANG X., LI L., YUAN A., PAN J. Superb VOCs capture engineering carbon adsorbent derived from shaddock peel owning uncompromising thermal-stability and adsorption property. Chinese Journal of Chemical Engineering, **47**, 120, **2022**.

46. LI N., YE J., DAI H., SHAO P., LIANG L., KONG L., YAN B., CHEN G., DUAN X. A critical review on

correlating active sites, oxidative species and degradation routes with persulfate-based antibiotics oxidation. Water Research, **235**, 119926, **2023**.

47. HUNG C-M., CHEN C-W., HUANG C-P., DONG C-D. Metal-free single heteroatom (N, O, and B)-doped coconut-shell biochar for enhancing the degradation of sulfathiazole antibiotics by peroxymonosulfate and its effects on bacterial community dynamics. Environmental Pollution, **311**, 119984, **2022**.

48. HUONG P.T., JITAE K., AL TAHTAMOUNI T.M., LE MINH TRI N., KIM H-H., CHO K.H., LEE C. Novel activation of peroxymonosulfate by biochar derived from rice husk toward oxidation of organic contaminants in wastewater. Journal of Water Process Engineering, **33**, 101037, **2020**.

49. HUNG C-M., HUANG C-P., CHEN C-W., WU C-H., LIN Y-L., DONG C-D. Activation of percarbonate by water treatment sludge–derived biochar for the remediation of PAH-contaminated sediments. Environmental Pollution, **265**, 114914, **2020**.

50. LIN X., CHEN Y., ZHOU D., CHEN M., LIANG W., GUO H. Aminated graphene quantum dots/CdS nanobelts for enhanced photocatalytic degradation of RhB dye under visible light. RSC Advances, **14** (1), 255, **2024**.

51. FAROOQ U., DANISH M., LYU S., BRUSSEAU M. L., GU M., ZAMAN W. Q., QIU Z., SUI Q. The impact of surface properties and dominant ions on the effectiveness of G-nZVI heterogeneous catalyst for environmental remediation. Science of The Total Environment, **651**, 1182, **2019**.

52. MISERLI K., KOGOLA D., PARASCHOUDI I., KONSTANTINOU I. Activation of persulfate by biochar for the degradation of phenolic compounds in aqueous systems [J]. Chemical Engineering Journal Advances, **9**, 100201, **2022**.

53. SEPTIAN A., KUMAR A.V.N., SIVASANKAR A., CHOI J., HWANG I., SHIN W.S. Colloidal activated carbon as a highly efficient bifunctional catalyst for phenol degradation. Journal of Hazardous Materials, **414**, 125474, **2021**.

54. LI F., DUAN F., JI W., GUI X. Biochar-activated persulfate for organic contaminants removal: Efficiency, mechanisms and influencing factors. Ecotoxicology and Environmental Safety, **198**, 110653, **2020**.

55. FANG G., ZHU C., DIONYSIOU D.D., GAO J., ZHOU D. Mechanism of hydroxyl radical generation from biochar suspensions: Implications to diethyl phthalate degradation. Bioresource Technology, **176**, 210, **2015**.

56. ZHONG D., JIANG Y., ZHAO Z., WANG L., CHEN J., REN S., LIU Z., ZHANG Y., TSANG D. C.W., CRITTENDEN J.C. pH Dependence of Arsenic Oxidation by Rice-Husk-Derived Biochar: Roles of Redox-Active Moieties. Environmental Science & Technology, **53** (15), 9034, **2019**.

57. PAN X., GU Z., CHEN W., LI Q. Preparation of biochar and biochar composites and their application in a Fenton-like process for wastewater decontamination: A review. Science of The Total Environment, **754**, 142104, **2021**.

58. TANG R., GONG D., DENG Y., XIONG S., ZHENG J., LI L., ZHOU Z., SU L., ZHAO J. π-π stacking derived from graphene-like biochar/g-C$_3$N$_4$ with tunable band structure for photocatalytic antibiotics degradation via peroxymonosulfate activation. Journal of Hazardous Materials, **423**, 126944, **2022**.

59. HU Y., CHEN D., ZHANG R., DING Y., REN Z., FU M., CAO X., ZENG G. Singlet oxygen-dominated activation of peroxymonosulfate by passion fruit shell derived biochar for catalytic degradation of tetracycline through a non-radical oxidation pathway. Journal of Hazardous Materials, **419**, 126495, **2021**.

60. LI X., JIA Y., ZHOU M., SU X., SUN J. High-efficiency degradation of organic pollutants with Fe, N co-doped biochar catalysts via persulfate activation. Journal of Hazardous Materials, **397**, 122764, **2020**.

61. YAN J., QIAN L., GAO W., CHEN Y., OUYANG D., CHEN M. Enhanced Fenton-like Degradation of Trichloroethylene by Hydrogen Peroxide Activated with Nanoscale Zero Valent Iron Loaded on Biochar. Scientific Reports, **7** (1), 43051, **2017**.

62. OUYANG D., YAN J., QIAN L., CHEN Y., HAN L., SU A., ZHANG W., NI H., CHEN M. Degradation of 1,4-dioxane by biochar supported nano magnetite particles activating persulfate. Chemosphere, **184**, 609, **2017**.

63. MIAN M.M., LIU G., FU B., SONG Y. Facile synthesis of sludge-derived MnOx-N-biochar as an efficient catalyst for peroxymonosulfate activation. Applied Catalysis B: Environmental, **255**, 117765, **2019**.